https://doi.org/10.36296/1819-8058.2025.3(82).115-124

INFLUENCE OF ELECTRO-THERMAL PARAMETERS OF POLYMER COMPOSITE FUSES ON THE EFFICIENCY OF SOLAR CELLS

Received Jun. 09, 2025; accepted Sept. 22, 2025
Available online Sept. 30, 2025

Korsunskyi R.[1], Nakashydze L.[2]

Author for correspondence: Nakashydze Lilia,
e-mail: foton_dnu@ukr.net

[1] student
https://orcid.org/0009-0001-5361-0641

[2] Dr. of Science (Tech.)
https://orcid.org/0000-0003-3990-6718

[1] The Stony Brook School, New York, USA

[2] Oles Honchar Dnipro National University, Research Institute of Energy-Efficient Technologies and Materials Science, Dnipro, Ukraine

Annotation: A solar cell system integrated with a conductive polymer composite fuse (CPCF) for passive protection against hot spot formation was numerically investigated. The model, based on differential heat balance equations, simulates diurnal temperature and power dynamics for Stony Brook, NY, on September 3rd, when the fuse is in the high-conductivity state, by considering heat exchange between the solar cell and the CPCF under varying solar irradiance and ambient conditions. Key material and structural parameters—such as thermal contact resistance, CPCF thickness, activation energy, percolation pre-exponential factor, and transition exponent—are varied to evaluate their influence on system performance. Results demonstrate that thermal contact resistance significantly influences temperature distribution between components without substantially affecting power output, while electrical parameters such as activation energy and percolation constants significantly influence power dissipation and overall energy loss. The findings provide a framework for optimizing CPCF design to enhance solar cell reliability and efficiency, offering a cost-effective, passive alternative to conventional hotspot mitigation methods.

Keywords: *solar cell, conductive polymer composite fuse, percolation, nanofiller, polymer matrix.*

ВПЛИВ ЕЛЕКТРОТЕПЛОВИХ ПАРАМЕТРІВ ПОЛІМЕРНИХ КОМПОЗИТНИХ ЗАПОБІЖНИКІВ НА ЕФЕКТИВНІСТЬ СОНЯЧНИХ ЕЛЕМЕНТІВ

Отримано 09 черв. 2025 р.; рекомендовано до публікації 22 вер. 2025 р.
Доступно онлайн 30 вер. 2025 р.

Корсунський Р. Д.[1], Накашидзе Л. В. [2]

Автор для кореспонденції: Накашидзе Лілія,
e-mail: foton_dnu@ukr.net

[1] студент
https://orcid.org/0009-0001-5361-0641

[2] д-р. техн. наук
https://orcid.org/0000-0003-3990-6718

[1] Школа Стоуні-Брук, Нью-Йорк, США

[2] Дніпровський національний університет імені Олеся Гончара, Науково-дослідний інститут енергоефективних технологій та матеріалознавства, м. Дніпро, Україна

Анотація: Було чисельно досліджено сонячний елемент, інтегрований з провідним полімерно-композитним запобіжником для пасивного захисту від утворення гарячих точок. Математична модель, заснована на диференціальних рівняннях теплового балансу, моделює фізичні процеси в цій системі для Стоуні-Брук, штат Нью-Йорк, 3 вересня, коли запобіжник перебуває у стані високої провідності, враховуючи теплообмін між сонячною батареєю та запобіжником за змінної сонячної радіації та умов навколишнього середовища. Ключові параметри матеріалу та конструкції, як-от термічний контактний опір, товщина матеріалу запобіжника, енергія активації запобіжника, передекспоненціальний коефіцієнт перколяції та показник перколяційного переходу, змінюються, щоб оцінити, як запобіжник впливає на продуктивність системи. Результати демонструють, що термічний контактний опір суттєво впливає на розподіл температури між компонентами без істотного впливу на вихідну потужність, тоді як електричні параметри, як-от енергія активації та константи перколяції, суттєво впливають на розсіювання потужності та загальні втрати енергії. Отримані результати

забезпечують основу для оптимізації конструкції запобіжників для підвищення надійності та ефективності сонячних елементів, пропонуючи економічно ефективну пасивну альтернативу звичайним методам захисту від впливу гарячих точок.

Ключові слова: *сонячний елемент, електропровідний полімерно-композитний запобіжник, перколяція, наповнювач, полімерна матриця.*

List of Abbreviations and Symbols

SC – *solar cell* PVC – *photovoltaic cell*

CPCF – *conductive polymer composite fuse* BDF – *backwards differentiation formula*

Introduction

Interest in renewable energy sources continues to grow steadily around the world. According to the Global Electricity Review conducted by the think tank Ember [1], renewable energy sources supplied a record 30% of the world's electricity, largely due to the increasing use of solar energy. Various defects that arise during solar cell (SC) operation lead to mismatches in photovoltaic characteristics between individual SCs and their series-connected groups. As a result, localized electrical overheating occurs within SCs, known as a "hot spot," which accelerates degradation processes [2].

In [3], the main causes of SC degradation and failure were analyzed, identifying hot spots as the source of 22% of faults. Therefore, one of the key directions for improving the reliability and efficiency of SCs is the study and development of technologies for protection against localized overheating.

Modern methods of preventing hot spot formation in SCs—including the use of bypass diodes and various circuit-based techniques—are not universal. Bypass diodes play a critical role in preventing mismatch effects, but they lead to technical challenges such as overheating, replacement needs, potential failures, and increased manufacturing costs due to the requirement of multiple diodes per SC series string [4–6]. Similarly, active bypass switches use field-effect transistors and can replace conventional bypass diodes, allowing more efficient bypass current flow and significantly reducing voltage drops [7]. In addition, some active detection systems use thermal images and temperature sensors to detect hot spots, subsequently activating integrated bypass switch systems to mitigate them [8]. However, these advanced methods often result in high costs and significantly complicate the solar installation.

In [9], a method was proposed for protecting SCs from localized overheating using a conductive polymer composite fuse (CPCF) as an embedded layer, maintaining thermal contact with the SC. In [10], modeling of the electrophysical characteristics of the system proposed in [9] was carried out using a polyethylene–carbon nanomaterial as a fuse. The possibility of applying this model for SC protection was analyzed, and directions for optimizing fuse parameters in protection circuits were identified. It was shown that currently available CPCFs have limited applicability for preventing localized SC overheating.

A study [11] demonstrated that the melting points of most commercially produced CPCFs are too high compared to the maximum operating temperatures of SCs and hot spot conditions. In [12], the possibility of creating CPCFs using a ceresin matrix—which has a lower melting point than most polyesters—combined with carbon black, was presented. Additionally, current research addresses the temperature distribution in the proposed model under overvoltage conditions [13]. Theoretical analysis in [13] shows that under such conditions, the local heating zone of a solar panel expands over time, causing the posistor layer to heat above its melting point.

Thus, the limitations and potential advantages of using a built-in posistor polymer composite layer for electrothermal protection of SCs were outlined earlier.

Methods and Results of the Study

To analyze the thermal behavior of a solar cell thermally coupled with a polymer-composite fuse, a mathematical model was developed based on a system of first-order differential equations describing the temperature dynamics of both components in thermal contact.

The heat balance for the solar cell is given by:

$$S_s A_s q(t) - S_s h_s \theta_s(t) - \frac{\theta_s(t)-\theta_p(t)}{R_{sp}} = S_s \rho_s c_{ps} l_s \frac{d\theta_s(t)}{dt} \quad (1)$$

where: $S_s A_s q(t)$ represents heat generation due to solar irradiance; $S_s h_s \theta_s(t)$ is heat loss to the surroundings; $\frac{\theta_s(t)-\theta_p(t)}{R_{sp}}$ models heat transfer between the solar cell and CPCF via thermal resistance R_{sp}; $S_s \rho_s c_{ps} l_s \frac{d\theta_s(t)}{dt}$ represents the heat capacity of the solar cell.

When creating the model, it was assumed that the CPCF samples consisted of an isotropic mechanical mixture of polymer matrix and conductive nanofiller.

The heat balance for the polymer-composite fuse is:

$$\frac{\theta_s(t)-\theta_p(t)}{R_{sp}} - S_p h_p \theta_p(t) + P(t) = S_p \rho_p c_{pp} l_p \frac{d\theta_p(t)}{dt} \quad (2)$$

where: $S_p h_p \theta_p(t)$ accounts for heat loss to the surroundings; $\frac{\theta_s(t)-\theta_p(t)}{R_{sp}}$ represents thermal conduction from the solar cell; $S_p \rho_p c_{pp} l_p \frac{d\theta_p(t)}{dt}$ describes the heat capacity of the

CPCF; $P(t)$ is power dissipation on the layer of the CPCF due to current flow.

In deriving the heat balance equation for the CPCF, it was assumed that the thermal properties of the composite material are primarily determined by the polymer matrix, while the contribution of the filler to heat transfer was not explicitly considered. This assumption is justified by the fact that polyethylene, as the dominant phase in the composite, largely determines the overall thermal behavior of the material.

The temperature excesses of the solar cell and the CPCF are defined as:

$$\theta_s(t) = T_s(t) - T_a(t) \quad (3)$$

$$\theta_p(t) = T_p(t) - T_a(t) \quad (4)$$

where T_s and T_p are the temperatures of the solar cell and CPCF, respectively; while T_a is the ambient temperature. The ambient temperature is approximated as a sinusoidal function of time:

$$T_a(t) = A_{temp} sin\left(\frac{2\pi}{24}t + t_{shift}\right) \quad (5)$$

where A_{temp} is the amplitude of temperature variation, and t_{shift} accounts for phase shifts in the daily temperature cycle.

This model is characterized by the following parameters:

- Geometric dimensions: surface areas S_s and S_p with corresponding thicknesses l_s and l_p.
- Material properties: densities ρ_s and ρ_p, and specific heat capacities c_{ps} and c_{pp}.
- Thermal characteristics: convective heat transfer coefficients h_s and h_p, solar absorption coefficient A_s, and interfacial thermal contact resistance R_{sp}.

Equations (1) and (2) can be rewritten as:

$$\frac{d\theta_s(t)}{dt} = \frac{1}{\alpha_s}(\beta_s q(t) - \gamma_s \theta_s(t) + \delta_s \theta_p(t)) \quad (6)$$

$$\frac{d\theta_p(t)}{dt} = \frac{1}{\alpha_p}(P(t) - \gamma_p \theta_p(t) + \delta_p \theta_s(t)) \quad (7)$$

where:

$$\alpha_s = S_s \rho_s c_{ps} l_s;$$

$$\beta_s = S_s A_s;$$

$$\gamma_s = S_s h_s + \frac{1}{R_{sp}};$$

$$\delta_s = \frac{1}{R_{sp}};$$

$$\alpha_p = S_p \rho_p c_{pp} l_p;$$

$$\gamma_p = S_p h_p + \frac{1}{R_{sp}} \text{ and } \delta_p = \frac{1}{R_{sp}}.$$

To describe the process of the CPCF's influence on the SC, a model of power dissipation and percolation conductivity is presented. It is based on the assumption that the power dissipation in the CPCF is determined by the short-circuit photocurrent I_{sc} and the fuse's temperature-dependent resistance R_p according to Joule's heating law:

$$P(t) = {I_{sc}}^2 * R_p \quad (8)$$

The resistance of the CPCF depends on its thickness, cross-sectional area, and conductivity:

$$R_p = \frac{l}{\sigma(T_p) * S_{cs}} \quad (9)$$

where: $\sigma(T_p)$ is the conductivity of the CPCF, which can be obtained from the percolation theory of conductance for materials that undergo a metal-dielectric transition [14]:

$$\begin{cases} \sigma(\Delta T_p) = A * exp^{\frac{-\Delta E}{kT_p}} \left(\frac{V_f(\Delta T_p) - V_c}{1 - V_c}\right)^t, & T_p < T_c \\ \sigma(\Delta T_p) = \sigma_m \left(\frac{A * exp^{\frac{-\Delta E}{kT_p}}}{\sigma_m}\right)^s, & T_p = T_c \\ \sigma(\Delta T_p) = \sigma_m \left(\frac{V_c - V_f(\Delta T_p)}{V_c}\right)^{-q}, & T_p > T_c \end{cases} \quad (10)$$

where: $\Delta T_p = T_p - T_0$, and T_0 is the initial ambient temperature; V_f is the volume fraction of a filler:

$$V_f(\Delta T_p) = \frac{1}{1 + \frac{(1 - V_{f0})(1 + \beta_m \Delta T_p)}{V_{f0}(1 + \beta_f \Delta T_p)}} \quad (11)$$

where: V_{f0} is the volume of a filler at initial conditions, and β_f and β_m are the coefficients of thermal expansion of the filler and matrix, respectively. T_c is the critical temperature of phase transition, determined from the equality $V_f(\Delta T_p) = V_c$. The constants $t, s,\ q$, and ΔE depend on the fuse material properties [13].

An important component of approximation is the effect of variable solar irradiance. According to the formula derived in [15], the introduced distribution is expressed through the duration of the local day t_d and the maximum values of the daily received irradiance q_{max}. Solar radiation on a horizontal surface depends on the degree of symmetry relative to the point $t = t_{max}$, at which the received solar irradiance reaches its maximum values. In the developed mathematical model, the distribution is assumed to be symmetric around the point $t_{max} = \frac{t_d}{2}$, which leads to the following expression:

$$q(t) = q_{max} \left(\frac{t}{t_{max}}\right)^2 \left(\frac{t_d - t}{t_d - t_{max}}\right)^2 \quad (12)$$

The length of the day t_d can be approximated in terms of latitude φ and the solar declination angle δ as follows:

$$t_d = \frac{24}{180^\circ} arcco\, s(tan\varphi\ tan\delta) \quad (13)$$

and formula for solar inclination angle is:

$$\delta = 23.45 sin 360 \left(\frac{284 + n}{365}\right) \quad (14)$$

Here, n is the day of the year starting from January 1st.

An integral part of the mathematical model is the inclusion of a description for determining the temperature-dependent photovoltaic characteristics for calculating the power

generation of solar energy. The mathematical model employs a dependence that describes the short-circuit current density of the solar cell as a function of the solar cell temperature and solar irradiance [16]:

$$J_{sc} = e * Q\big(1 - R_c(T_s)\big)(1 - exp^{-\mu l})\frac{q(t)}{E_g} \qquad (15)$$

where: elementary charge is denoted by *e*, and *Q* represents the collection factor of the solar cell. The reflection coefficient of the front surface of the solar cell, R_c, is given by the equation:

$$R_c(T_s) = 0.322 + 3.12 * 10^{-5} T_s \qquad (16)$$

where: T_s is the absolute temperature of the surface of the solar cell (under zero gradient conditions); μ is the attenuation coefficient, and the value is given as:

$$\mu = ae^{\frac{T_S}{\tau}} \qquad (17)$$

where $a = 3.17 \times 10^4$ and $\tau = 346K$. The variable l (in meters) represents the thickness of the solar cell [16].

The energy band gap for the semiconductor is given as [16]:

$$E_g = E_g(0) - \frac{\alpha {T_s}^2}{T_s + \beta} \qquad (18)$$

For silicon: $E_g(0) = 1.16eV$, $\alpha = 7 \times 10^{-14} eV \cdot K^{-1}$ and $\beta = 1100K$.

The open circuit voltage V_{oc} is defined as [16]:

$$V_{oc} = \frac{KT_s}{e} ln\left(\frac{J_{sc}}{J_0} + 1\right) \qquad (19)$$

where: the Boltzmann constant is denoted by *K*, and *e* represents the elementary charge. The reverse saturation current density, J_0 , depends on temperature as follows [15]:

$$J_0 = \varepsilon n {T_s}^{\gamma} ex\, p\left(\frac{-E_g}{KT_s}\right) \qquad (20)$$

where $\varepsilon = 179 \frac{A}{K^3 m^2}$ for a silicon solar cell; n is a non-ideality factor taken as $n = 1$, and $\gamma = 3$ [15].

The silicon solar cell is considered with dimensions of 156mm × 156mm × 3.5mm.

The solar absorption coefficient A_s is taken as 0.8. Convective heat transfer coefficients for both SC and CPCF are taken as $h_s = h_p = 20\ \frac{W}{m^2 K}$. The density and specific heat capacity of silicon are:

$$\rho_s = 2280\ \frac{kg}{m^3},\ c_{ps} = 840\ \frac{J}{kg*K}\ .$$

The distribution of diurnal solar radiation is considered for Stony Brook, New York, as an example. For Stony Brook on September 3, the corresponding parameters for estimating solar radiation distribution are: $q_{max} = 850\ \frac{W}{m^2}$, $n = 245$, $\varphi = 40.9257°$.

The length of the local daytime is approximated to be $t_d \approx 12.5h$, and the time corresponding to maximum solar radiation is $t_{max} = 6.25\ h$. The amplitude of the ambient temperature variation is taken as $A_{temp} = 12°C$, while the time shift is considered to be 0.

The presence of CPCF in the electrical circuit should not affect the normal operation of the system. Therefore, there are two requirements for CPCF selection [10]: the internal resistance of the solar cell r must be significantly higher than the minimal initial resistance of the CPCF, i.e., r $\gg$ R_{min}; the short-circuit current of the solar cell must not exceed the triggering current I_{trip} of the CPCF, i.e., $I_{trip} > I_{sc}$.

The volume fraction of the filler V_{f0} at initial conditions is 0.23, while the critical volume fraction V_c is 0.14. This results in a critical temperature of the CPCF $T_c = 114°C$.

Percolation exponents were assigned as follows: $s = 0.62$, and $q = 1$ [10].

The thermal expansion coefficients of the polyethylene matrix and the filler were:

$\beta_m = 6.93 \times 10^{-3}\ \mathrm{K}^{-1}$, $\beta_f = 10^{-6}\ \mathrm{K}^{-1}$, respectively [13]. Additionally, the thermal conductivity of the matrix was given as $\sigma_m = 5 \times 10^{-14}\ \frac{W}{m*K}$.

The computations were performed using Python within the PyCharm integrated development environment. The system of differential equations was numerically solved using the backward differentiation formula (BDF) method from the scipy.integrate library. The BDF method was chosen due to the stiffness of the first-order differential equations in this study, ensuring solution stability.

To compute the area between curves, the composite Simpson's rule was applied, providing a reasonable approximation. This was implemented using the Simpson function from scipy.integrate.

The simulations analyze the thermal response of the CPCF-integrated solar cell under varying diurnal sunlight conditions, considering factors such as ambient temperature fluctuations, power dissipation, and solar irradiance distribution. The results show the temperature dynamics of both the solar cell and the CPCF. Additionally, the total power output of the system, power generated by the solar cell, and power dissipated on the CPCF are calculated for different values of contact thermal resistance (R_{sp}), and various CPCF material properties such as: preexponential coefficient A, activation energy ΔE, percolation transition exponent t, and thickness l_p.

First, simulations were conducted with four different values of thermal resistance R_{sp} to analyze the thermal behavior of the system. The corresponding CPCF material properties were applied and held constant, including the percolation exponent $t = 1.2$ for the metal-conductive state of CPCF, the pre-exponential coefficient $A = 1200$ in the metal-conductive state, and the activation energy $\Delta E = 9.72 \times 10^{-21}$ J. Additionally, the CPCF layer thickness was set to $l_p = 0.002m$. Equation (21) was used to calculate the energy loss.

$$E_{loss} = \int_0^{t_d} P_{gen} dt - \int_0^{t_d} P_{total} dt \qquad (21)$$

Table 1 presents a comparison of the results obtained for four different values of thermal contact resistance: $0.1\ \frac{^\circ C}{W}$, $0.5\ \frac{^\circ C}{W}$, $1.0\ \frac{^\circ C}{W}$, and $1.5\ \frac{^\circ C}{W}$. Knowing the temperatures of both CPCF and SC at each point in time enabled the calculation of solar cell power generation and power dissipation in CPCF.

To illustrate the temperature dynamics for different thermal contact resistance values, Fig. 1 was generated based on solved differential equations.

Table 1. Temperature and power distributions for 4 different values of contact thermal resistance R_{sp}

Parameter	R_{sp} = 0.1 $\frac{^\circ C}{W}$	R_{sp} = 0.5 $\frac{^\circ C}{W}$	R_{sp} = 1.0 $\frac{^\circ C}{W}$	R_{sp} = 1.5 $\frac{^\circ C}{W}$
T_s at $t = t_{max}$ *(°C)*	41.4	42.8	44.3	45.5
T_p at $t = t_{max}$ *(°C)*	40.6	39.1	37.7	36.4
Total Energy Generation, E_{gen} *(Wh)*	26.3	26.2	26.2	26.1
Total Energy Loss, E_{loss} *(Wh)*	1.7	1.7	1.8	1.7
Total System Output, E_{total} *(Wh)*	24.6	24.5	24.4	24.4

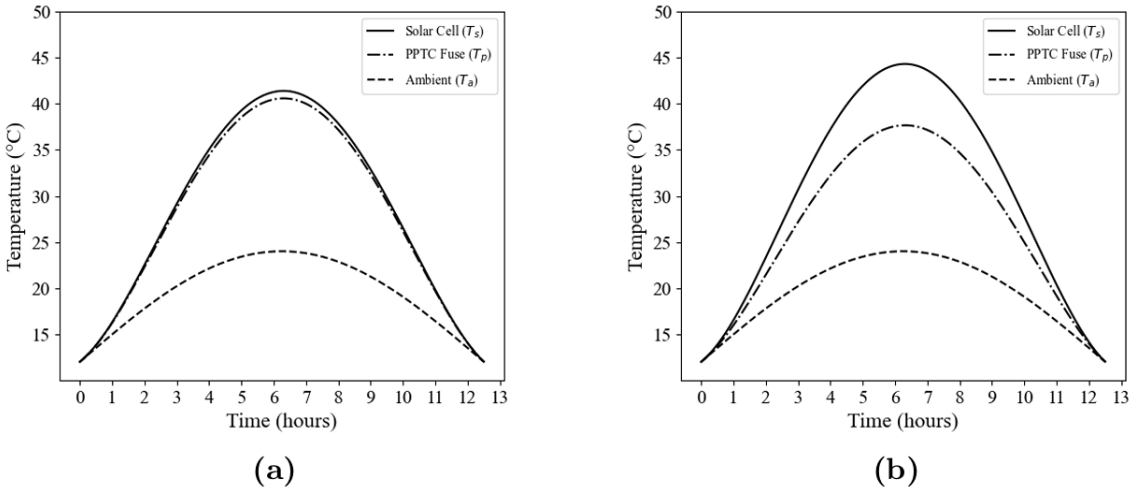

Fig. 1. Temperature dynamics for different values of contact thermal resistance (R_{sp}) between layers of SC and CPCF. (a) $R_{sp} = 0.1\ \frac{^\circ C}{W}$, (b) $R_{sp} = 1.0\ \frac{^\circ C}{W}$

Next, the power output analysis of the model was conducted based on 4 varying thickness values: 1mm, 2mm, 3mm, 4mm. The results are shown in Table 2. The corresponding simulation parameters included thermal contact resistance $R_{sp} = 0.5\frac{^\circ C}{W}$, exponent $t = 1.2$ for the metal-conductive state of CPCF, pre-exponential coefficient $A = 1200$ in the metal-conductive state, and activation energy $\Delta E = 9.72 \times 10^{-21}$ J.

Lastly, a variety of material constants were examined. Fig. 2 illustrates the dependence of CPCF resistance on temperature for two different values of percolation exponent t (equation 10). Graphs were obtained for a logarithmic scale of resistance.

For this simulation, thermal contact resistance R_{sp} was set to $0.5\frac{^\circ C}{W}$, pre-exponential coefficient A = 1200, activation energy $\Delta E = 9.72 \times 10^{-21}$ J and CPCF layer thickness $l_p = 0.002m$. Four different values of the percolation transition exponent t were studied. The percolation exponent plays a crucial role in defining how conductivity changes as the filler concentration approaches the percolation threshold. By varying t, it is possible to assess the sensitivity of the system's power distribution to changes in the conductive network structure. Table 3 illustrates how four different values of t affect the power distribution of the system.

Fig. 3 illustrates the power distribution for two different values of the percolation transition exponent t.

Table 2. Temperature and power distributions for 4 different values of CPCF thickness l_p

Parameter	l_p = 0.001m	l_p = 0.002m	l_p = 0.003m	l_p = 0.004m
T_s at $t = t_{max}$ *(°C)*	42.8	42.8	42.8	42.8
T_p at $t = t_{max}$ *(°C)*	39.2	39.1	39.1	39.1
Total Energy Generation, E_{gen} *(Wh)*	30.0	30.0	30.0	30.0
Total Energy Loss, E_{loss} *(Wh)*	1.9	3.9	5.8	7.8
Total System Output, E_{total} *(Wh)*	28.1	26.1	24.2	22.2

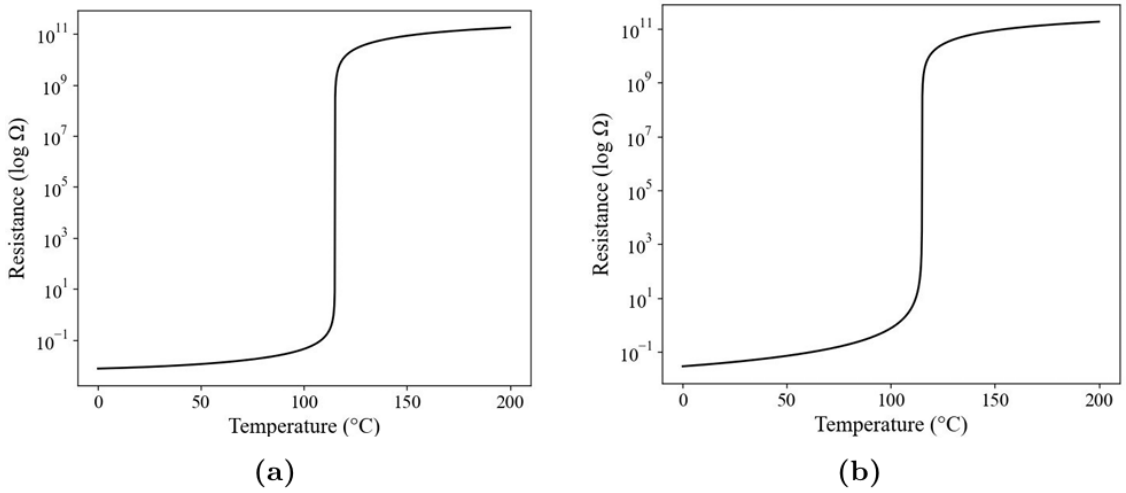

Fig. 2. Variation of the CPCF resistance as a function of temperature for two values of t. (a) $t = 1.0$, (b) $t = 1.6$

Table 3. Temperature and power distributions for 4 different values of percolation transition exponent t

Parameter	t = 1.0	t = 1.2	t = 1.4	t = 1.6
T_s at $t = t_{max}$ *(°C)*	42.8	42.8	42.8	42.8
T_p at $t = t_{max}$ *(°C)*	39.1	39.2	39.2	39.2
R_p at $t = 0$ *(Ω)*	0.010	0.018	0.29	0.050
R_p at $t = t_{max}$ *(Ω)*	0.012	0.021	0.037	0.067
Total Energy Generation, E_{gen} *(Wh)*	30.0	30.0	30.0	30.0
Total Energy Loss, E_{loss} *(Wh)*	2.2	3.9	6.9	12.2
Total System Output, E_{total} *(Wh)*	27.8	26.1	23.1	17.8

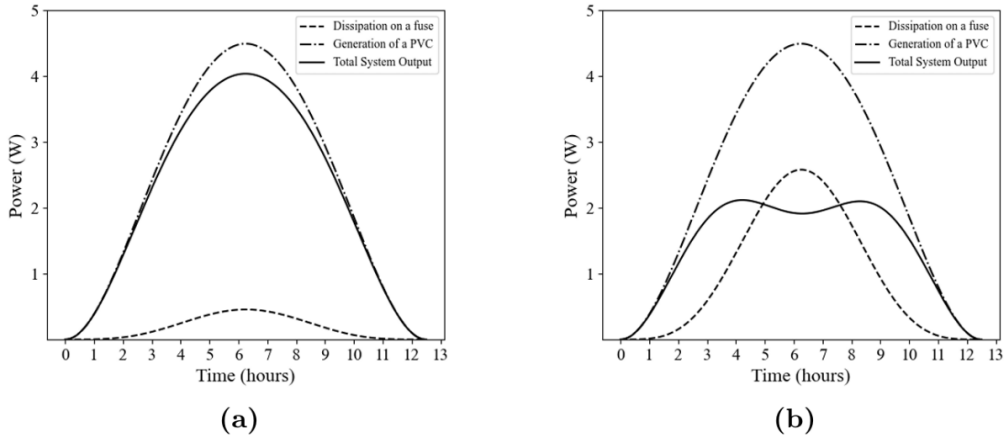

Fig. 3. Power distribution at the system throughout the solar hours for two values of t. (a) $t = 1.0$, (b) $t = 1.6$

For the following simulation, the thermal contact resistance R_{sp} was set to $0.5\frac{^{\circ}C}{W}$, the activation energy $\Delta E = 9.72 \times 10^{-21}$ J, percolation transition exponent $t = 1.2$, and the CPCF layer thickness $l_p = 0.002m$. The pre-exponential coefficient A was varied across multiple values to study its effect on the system's power distribution. The pre-exponential factor, commonly denoted as A, serves as a coefficient in the percolation theory conductivity equation, which characterizes how the preexponential factor relates directly to the frequency of successful collisions between charge carriers in the conductive network. Table 4 presents the impact of different values of A on the power distribution of the system, illustrating how variations in this parameter affect thermal and electrical performance.

Then, different values of CPCF activation energy were studied. The thermal contact resistance R_{sp} was set to $0.5\frac{^{\circ}C}{W}$, pre-exponential coefficient $A = 1200$, percolation transition exponent $t = 1.2$, and the CPCF layer thickness l_p= 0.002m. The activation energy ΔE was varied across multiple values to study its effect on the system's power distribution. The activation energy of a CPCF is the minimum thermal energy required to initiate a significant increase in the material's electrical resistance due to the disruption of the conductive network within the polymer matrix. This

energy corresponds to the temperature-dependent processes such as polymer expansion, filler debonding, or phase transitions driving the material from a conductive into a high-resistance (fused) state.

Table 4. Temperature and power distributions for 4 different values of percolation pre-exponential coefficient A

Parameter	A = 250	A = 500	A = 900	A = 1200
T_s at $t = t_{max}$ *(°C)*	42.8	42.8	42.8	42.8
T_p at $t = t_{max}$ *(°C)*	39.1	39.1	39.1	39.1
R_p at $t = 0$ *(Ω)*	0.077	0.042	0.023	0.018
R_p at $t = t_{max}$ *(Ω)*	0.101	0.050	0.028	0.021
Total Energy Generation, E_{gen} *(Wh)*	30.0	30.0	30.0	30.0
Total Energy Loss, E_{loss} *(Wh)*	18.8	9.4	5.2	3.9
Total System Output, E_{total} *(Wh)*	11.1	20.6	24.8	26.1

Table 5 presents the temperature and power distribution of the system with varying values of activation energy ΔE.

The numerical simulations revealed several important insights regarding the influence of key parameters on system performance, which are discussed in detail below.

Thermal contact resistance (R_{sp}) at the interface between a solar cell and a polymer composite layer is influenced by multiple factors, including surface roughness, contact pressure, material properties, and interfacial air gaps [17]. The range of $0.1 - 1.5\frac{^{\circ}C}{W}$ used in this study appropriately includes both ideal conditions (lower R_{sp} values) and more challenging interface scenarios (higher R_{sp} values) that might occur in practical applications. This range allows for comprehensive analysis of how thermal contact resistance affects temperature distribution and system performance across various manufacturing and installation conditions, providing valuable insights for optimizing the thermal design of CPCF-integrated SCs.

Table 5. Temperature and power distributions for 4 different values of CPCF activation energy ΔE

Parameter	ΔE = 4.80× 10^{-21}J	ΔE = 9.72× 10^{-21}J	ΔE = 12.8× 10^{-21}J	ΔE = 16.2× 10^{-21}J
T_s at $t = t_{max}$ *(°C)*	42.8	42.8	42.8	42.8
T_p at $t = t_{max}$ *(°C)*	39.1	39.1	39.1	39.1
R_p at $t = 0$ *(Ω)*	0.005	0.018	0.037	0.082
R_p at $t = t_{max}$ *(Ω)*	0.007	0.021	0.043	0.091
Total Energy Generation, E_{gen} *(Wh)*	30.0	30.0	30.0	30.0
Total Energy Loss, E_{loss} *(Wh)*	1.2	3.9	8.1	17.4
Total System Output, E_{total} *(Wh)*	28.8	26.1	21.9	12.6

Discussions

The thermal contact resistance (R_{sp}) between the solar cell and CPCF layers significantly impacts the temperature distribution within the system. As shown in (Table 1), increasing R_{sp} from $0.1\frac{^{\circ}C}{W}$ to $1.5\frac{^{\circ}C}{W}$ resulted in higher solar cell temperatures (from 41.4°C to 45.5°C at maximum solar radiation) and lower CPCF temperatures (from 40.6°C to 36.4°C). This temperature change is critical for the proper functioning of the protection mechanism, as it determines how effectively heat is transferred from the solar cell to the CPCF layer. In other words, it defines the sensitivity of the CPCF.

The further analysis of thermal contact resistance (R_{sp}) reveals that while lower R_{sp} values result in higher CPCF temperatures, this temperature difference has a negligible effect on power dissipation and overall system performance. The energy loss remains nearly constant (1.7 − 1.8Wh) across all 4 cases. Therefore, increasing R_{sp} to reduce power dissipation on the CPCF appears unnecessary, as the thermal efficiency gains would be minimal. Instead, R_{sp} should be optimized primarily for protection sensitivity.

The temperature dynamics illustrated in Fig. 1 further demonstrate that higher thermal contact resistance creates a more pronounced temperature difference between the solar cell and CPCF. This characteristic could be advantageous in applications where a delayed response from the protection mechanism is desired, allowing for current to flow through without triggering the fuse. Conversely, in applications requiring rapid response to hot spots, lower thermal contact resistance would be preferable.

The thickness of the CPCF layer (l_p) emerged as a critical parameter affecting the system's electrical performance. As shown in Table 2, increasing the CPCF thickness from 1mm to 4mm had a dramatic effect on energy losses, which increased from 1.9Wh to 7.8Wh. Consequently, the total system output decreased significantly from 28.1Wh to 22.2Wh, representing a reduction of approximately 21 percent. This substantial impact on system performance can

be attributed to the increased electrical resistance of thicker CPCF layers, as resistance is directly proportional to length according to equation (9). The increased resistance leads to higher power dissipation during normal operation, reducing the overall efficiency of the system. The temperature behavior of both the solar cell and CPCF remained unchanged across different thickness values. This indicates that while thickness significantly affects electrical performance, its impact on thermal behavior is minimal under normal operating conditions of the CPCF. This finding suggests that CPCF thickness should be minimized to reduce energy losses while maintaining adequate protection capabilities.

While the numerical simulations in this study suggest that the most effective conductive polymer composite fuses for protecting 156 × 156mm solar cell wafers are approximately 1mm thick, the current manufacturing standards present a significant challenge. As demonstrated in Table 6 [18, 19, 20], commercial fuses, that satisfy fuse selection requirements for 156 x 156mm solar cell wafers established in the study [10], from leading manufacturers such as Littelfuse, Bourns, and Fuzetec typically range from 3.0 to 4.0mm in thickness, which is substantially thicker than the theoretically optimal size. This issue highlights a critical gap between theoretical optimization and current manufacturing capabilities. The thicker fuses, while readily available, may introduce additional energy losses and thermal inefficiencies that could compromise the overall performance of the solar cell protection system. However, it should be mentioned that the increased thickness of fuses from prominent manufacturers is not only due to the active fuse material but is also influenced by protective external shells and packaging requirements. Still, the findings show the need for advanced manufacturing techniques and material innovations that can produce thinner fuses identified as optimal in this study.

Table 6. Examples of fuse parameters that satisfy requirements for 156x156 mm solar cells [10]

Manufacturer	Model	Thickness (mm)	Trip Current (A)	Minimal Resistance (Ω)
Littelfuse	16R1400G	3.0	23.8	0.0026
	30R900U	3.0	18.0	0.0050
	AGRF1400	3.5	27.3	0.0022
Bourns	MFRHS1200	3.6	24.0	0.0035
	MFRHT1300	3.6	24.0	0.0041
	MFRHS900	3.6	18.0	0.0046
Fuzetec	FRU900-30F	3.0	18.0	0.0050
	FRG1200-16F	3.6	20.4	0.0020
	FHE1000-32F	4.0	20.0	0.0060

The percolation transition exponent t plays a crucial role in determining the temperature-dependent resistance characteristics of the CPCF. As illustrated in Fig. 2, higher values of t result in steeper resistance-temperature increase when the volume of the filler is higher than the percolation threshold, indicating greater sensitivity to temperature changes. This parameter influences how the conductive network within the polymer-composite responds to thermal variations. Our simulations showed that increasing t from 1.0 to 1.6 increased energy losses from 2.2Wh to 12.2Wh, resulting in a reduction in total system output from 27.8Wh to 17.8Wh (Table 3). This represents a decrease of approximately 36 percent in system efficiency. The power distribution curves shown in Figure 3 further illustrate that higher t values lead to increased power dissipation in the CPCF throughout the day. This behavior can be attributed to the more pronounced resistance increase with temperature at higher t values, resulting in greater Joule heating losses during normal operation. Materials with lower percolation transition exponents are preferable for CPCF applications in SCs, as they minimize energy losses during normal operation of the fuse.

The pre-exponential coefficient A in the percolation theory conductivity equation significantly influences the baseline conductivity of the CPCF. Our simulations demonstrated that increasing A from 250 to 1200 reduced the initial resistance (R_{min}) from 0.077Ω to 0.018Ω (Table 4), resulting in substantially lower energy losses (from 18.8Wh to 3.9Wh) and higher total system output (from 11.2Wh to 26.1Wh). This improvement in system performance with higher A values can be attributed to the reduced resistance of the CPCF, which minimizes power dissipation during normal operation. The pre-exponential coefficient determines the density of conductive pathways within the polymer matrix, with higher values indicating more efficient charge transport mechanisms. Materials with optimized filler dispersion and enhanced interfacial interactions between the conductive filler and polymer matrix, exhibiting higher A values, are promising candidates for this application.

The activation energy ΔE of the CPCF material defines the temperature sensitivity of its conductivity. Our simulations showed that increasing ΔE from 4.80×10^{-21} J (0.03eV) to 16.1×10^{-21} J (0.1eV) resulted in a substantial increase in initial resistance from 0.005Ω to 0.082Ω (Table 5). This led to dramatically higher energy losses (from 1.2Wh to 17.4Wh) and reduced total system output (from 28.8Wh to 12.6Wh), representing a decrease of approximately 56 percent. The significant impact of activation energy on system

performance can be explained by its exponential relationship with resistance. Higher activation energies result in greater temperature dependence of resistance, leading to increased power dissipation during normal operation as ambient and operating temperatures fluctuate throughout the day. These findings indicate that CPCF materials with lower activation energies are preferable for minimizing energy losses during normal operation.

Conclusions

The results of this study have several implications for the design and implementation of CPCF-based protection systems for solar cells. First, our findings highlight the importance of careful material selection and optimization. The electrical properties of the CPCF, particularly the percolation transition exponent, preexponential coefficient, and activation energy, have significant effects on system performance under normal conditions of operation (high-conductivity state of the CPCF) and must be carefully selected to balance protection capabilities with energy efficiency.

Second, the thickness of the CPCF layer should be minimized to reduce energy losses while maintaining adequate protection. This may require the development of novel manufacturing techniques capable of producing thin, uniform CPCF layers with consistent properties.

Third, the thermal contact resistance between the solar cell and CPCF layers should be optimized based on the specific requirements of the application. Lower thermal contact resistance may be preferable for applications requiring rapid response to hot spots, without compromising system efficiency.

Future research should focus on experimental validation of these numerical findings, particularly under hot spot conditions. Additionally, the development of CPCF materials with optimized properties for solar cell protection applications represents a promising field for future work. Finally, the integration of CPCF layers into commercial solar panels and the evaluation of their long-term reliability and performance under real-world conditions should be investigated.

In conclusion, this study provides insights into the thermal and electrical behavior of solar cells integrated with CPCF protection layers under varying diurnal sunlight conditions. The findings contribute to the development of more efficient and reliable solar energy systems by analyzing the key parameters affecting the performance of CPCF-based protection mechanisms.

REFERENCES

1. Ember. (2024). Global electricity review 2024. https://ember-energy.org/latest-insights/global-electricity-review-2024/
2. International Energy Agency Photovoltaic Power Systems Programme (IEA PVPS). (2014). Review of failures of photovoltaic modules: International Energy Agency PVPS Task 13.
3. Zhang, Z., Wang, L., et al. (2016). Study of bypass diode reliability under non-uniform irradiance distribution on PV module surface. Acta Energiae Solaris Sinica, 37(2), 355–360.
4. Fonseca Batista, R. V. (2018). The impact of shadowing in photovoltaic systems and how to minimize it: An analysis with the PVSyst software. https://www.diva-portal.org/smash/get/diva2:1214973/FULLTEXT01.pdf
5. Sullivan, R. M. (1965). Shadow effects on a series-parallel array of solar cells (NASA Technical Memorandum NASA-TM-X-55269). NASA Goddard Space Flight Center. https://ntrs.nasa.gov/api/citations/19650016433/downloads/19650016433.pdf
6. Vieira, R. G., de Araújo, F. M. U., Dhimish, M., & Guerra, M. I. S. (2020). A comprehensive review on bypass diode application on photovoltaic modules. Energies, 13(10), 2472. https://doi.org/10.3390/en13102472
7. d'Alessandro, V., Guerriero, P., & Daliento, S. (2013). A simple bipolar transistor-based bypass approach for photovoltaic modules. IEEE Journal of Photovoltaics, 4(1), 405–413.
8. Guerriero, P., Tricoli, P., & Daliento, S. (2019). A bypass circuit for avoiding the hot spot in PV modules. Solar Energy, 181, 430–438.
9. Tonkoshkur, A. S., Ivanchenko, A. V., Nakashydze, L. V., Lyashkov, A. Yu., & Gomilko, V. (2021). Application of polymer posistor nanocomposites in systems for protecting photovoltaic components of solar arrays from electrical overloads. Primedia eLaunch.
10. Lyashkov, A. Yu., Makarov, V. O., & Plakhtii, Y. G. (2022). Modeling of resettable fuses characteristics for protection of solar arrays from current overloads. Multidiscipline Modeling in Materials and Structures, 18(2), 328–338.
11. Tonkoshkur, A. S., Ivanchenko, A. V., Nakashydze, L. V., Lyashkov, A. Yu., & Gomilko, V. (2019). Posistor elements based on ceresin–nanocarbon composites. Journal of Physics and Electronics, 27(1), 71–78.
12. Tonkoshkur, A. S., & Ivanchenko, A. V. (2020). Modelling of overheating in solar photovoltaic cell plates with local electric heat sources. Journal of Physics and Electronics, 28(1), 77–84.
13. Zainutdinov, A. Kh., Kasymov, A. A., Alimov, R. A., & Magrupov, M. A. (1994). Influence of thermal expansion on the conductivity of polymer conducting composites. Journal of Engineering Physics and Thermophysics, 66(3).
14. El-Adawi, M. K. (2019). Prediction of symmetrical and asymmetrical global solar irradiance distribution—New approach. Optical and Photo Journal, 9, 15–24.
15. Shaban, S. S. M. (2020). The solar cell parameters as a function of its temperature in relation to its diurnal efficiency. Optics and Photonics Journal, 10, 1–12.

16. Singh, P., & Ravindra, N. M. (2012). Temperature dependence of solar cell performance—An analysis. Solar Energy Materials and Solar Cells, 101, 36–45.

17. Gibbins, J. (2006). Thermal contact resistance of polymer interfaces (Master's thesis). University of Waterloo, Ontario, Canada.

18. Littelfuse. (2025). Polyswitch resettable PPTC devices. Retrieved from https://www.littelfuse.com/products/fuses-overcurrent-protection/polyswitch-resettable-pptc-devices

19. "Multifuse Polymer PTC Resettable Fuses." Bourns. Retrived from www.bourns.com/products/circuit-protection/resettable-fuses-multifuse-pptc

20. "PPTC Resettable Fuse Product Catalog." Fuzetec. Retrived from www.fuzetec.com/upload/download/Fuzetec%202021%20PPTC%20Catalog.pdf